Optics Communications 517 (2022) 128278

Contents lists available at ScienceDirect

Optics Communications

journal homepage: www.elsevier.com/locate/optcom

Hybrid self-calibration method for reference surface elimination in subaperture stitching interferometry

WeiJian Liu [a], Zhishan Gao [a], Ruoyan Wang [a], Xiaoyu Che [a], Lingjie Wang [b], Lihua Lei [c], Zhenyan Guo [a], Qun Yuan [a,*]

[a] School of Electronic and Optical Engineering, Nanjing University of Science and Technology, Xiao Lingwei Road 200, Nanjing, Jiangsu, 210094, China
[b] Key Laboratory of Optical System Advanced Manufacturing Technology, Changchun Institute of Optics, Fine Mechanics and Physics, Chinese Academy of Sciences, Changchun 130033, China
[c] Shanghai Key Laboratory of Online Test and Control Technology, Shanghai 201203, China

ARTICLE INFO

Keywords:
Subaperture stitching
Wavefront interferometry
Error elimination

ABSTRACT

Subaperture stitching interferometry (SSI) is an essential method for the map testing of large-aperture optical components. The surface map of a reference surface is a typical error source. In this study, we propose a hybrid self-calibration method to eliminate the reference surface error in SSI by combining the modified shift-rotation method and the maximum likelihood method. The traditional shift-rotation method is a general full-aperture absolute interferometric measurement that can retain localized irregularities. The shift-rotation operations are leveraged to generate a couple of subapertures covering the surface under test, whereby a ring of subapertures and a central subaperture are acquired by rotations and a lateral shift, respectively. The modified shift-rotation method is proposed to obtain the rotationally asymmetric components of the test surface in the ring of subapertures. The same components within the central subaperture are retrieved using the maximum likelihood method. Then, the rotationally symmetric components of the test surface are acquired using the least squares method, utilizing the measured data before and after the shift. Reference surface maps are sufficiently eliminated from the measured data. High-frequency components of the test surface are also retained, which engender high-accuracy SSI. Simulations are conducted to verify the proposed method. The positioning errors of the proposed method are analysed and discussed. Subaperture testing experiments of a 100-mm aperture flat are performed and compared with full-aperture absolute measurement results. The stitched errors with 0.018 λ PV and 0.003 λ RMS are obtained.

1. Introduction

Interferometry is a general testing method for large-aperture optical elements. In interferometric testing, the reference aperture should at least be equal to the test optics, which involves high cost for testing large-aperture optics. Subaperture stitching interferometry (SSI) is a promising measurement method that eliminates the need of a large-aperture reference surface, which was first proposed by Kim and Wyant [1]. In the subaperture testing process, there are two ways to generate subapertures. The first one involves translating the test surface or reference surface along the X and Y axis, whereas the other one involves rotating the test surface. Mechanisms that induce surface shape deformations are non-negligible when testing a large aperture flat. Therefore, an appropriate method of generating subapertures needs to be selected to minimize the surface shape deformations in different interferometric systems. Considering that the surface gravity induces deformations, the X/Y translation operations can be used in both horizontal and vertical interferometric configurations, whereas the rotation operation is more suitable for SSI with a vertical interferometric configuration. Relative alignment errors, such as piston and tilt between adjacent subapertures, are calculated with least squares fit to the differences in the overlapping regions. Another factor called positioning error, which is induced by mechanical scanning, will introduce a mismatch of the corresponding points in the overlapping regions of two adjacent subapertures. Maurer and Zhang proposed marker point methods to eliminate the positioning errors [2,3]. In addition, Tang and Chen proposed algorithms to retrieve the positioning errors [4,5]. Reference surface errors are also important error sources that affect the accuracy of SSI.

In general, two schemes are applied to calibrate reference surfaces. The first one involves calibrating the reference surface with absolute measurements before conducting the stitching test, whereas the other one involves calibrating the reference surface during the stitching process. Absolute measurements, such as three-flat tests, the Zernike

* Corresponding author.
E-mail address: karmen86913@gmail.com (Q. Yuan).

https://doi.org/10.1016/j.optcom.2022.128278
Received 7 December 2021; Received in revised form 28 March 2022; Accepted 3 April 2022
Available online 16 April 2022
0030-4018/

polynomials fitting method and the even–odd function method, require three independent flats including two transmission flats and a flat under test [6–8]. These methods are complex and expensive.

QED Technologies proposed a self-calibration method [9]. Data consistency in the overlap region is used to reconstruct the reference surface described by Zernike polynomials. Then, the reference surface is removed from each subaperture during the stitching process. Su et al. proposed a maximum likelihood reconstruction method for testing a 1.6-m aperture flat [10,11]. Both the reference and test surfaces are rotated to reconstruct the reference surface and the test surface using Zernike polynomials. Yan et al. extended the maximum likelihood reconstruction method and proposed an orthonormal polynomial fitting method for testing a flat mirror with arbitrary shape [12]. In the above methods, high-frequency components of the reference surface are coupled with the test surface, since only the Zernike polynomial surface of the reference surface is calibrated during the stitching process. Owing to the higher testing accuracy, high-frequency components of the reference surface are expected to be eliminated during the stitching process. Chen et al. decomposed the reference surface into power, astigmatism, residual Zernike polynomial surface and high-frequency components, which are estimated and calibrated, respectively [13]. In this method, the power and astigmatism of the reference surface are measured with a modified three-flat testing method. The residual Zernike polynomial surface and high-frequency components of the reference surface are calibrated during the stitching process. This method is more suitable when the reference surface aperture is small since the three-flat testing method will be much more expensive when the reference surface aperture is large. In addition, the calculation of high-frequency components of the reference needs abundant subapertures, which also calls for a small-aperture reference surface. Kim et al. proposed a dual-subaperture stitching method to eliminate surface errors of the reference sphere in the Ritchey–Common test [14]. The test flat is decomposed into the surface form error and the rotationally symmetric (RS) components, such as power and spherical aberrations. The surface form error is acquired through rotations of the test flat, while the RS components are obtained by scanning along the centreline of the test flat. In this method, the diameter of the reference sphere needs to be larger than the semi-diameter of the test flat so that the surface form error can be calculated.

It is important to accurately calibrate the reference surface during the stitching process. The shift-rotation method, which requires shift and rotations of the test surface, involves general full-aperture absolute interferometric measurements and can retain localized irregularities. Since the subapertures generated by rotations are similar to those generated using the shift-rotation method, we suppose the latter method can be modified to eliminate the reference surface during the stitching process. In SSI, a ring of subapertures and a central subaperture are generated by rotations and a lateral shift. The modified shift-rotation method is applied to obtain the rotationally asymmetric (RAS) components of the test surface in the ring of subapertures. The absolute test surface in the central subaperture is calculated using the maximum likelihood method. Then, the RS components of the test surface can be acquired by applying the least squares method using the measured data before and after the shift. Therefore, a hybrid self-calibration method that is suitable for SSI with a vertical interferometric system is proposed to obtain the absolute test surface based on the combination of the modified shift-rotation method and the maximum likelihood method. The principle and procedure of the proposed method are elaborated in Section 2. In Section 3, simulations are conducted to verify the proposed method. Experimental results derived from the subaperture testing of a 100-mm aperture flat are presented in Section 4. Finally, Section 5 presents the conclusions.

2. Principle

The geometric setup of the subaperture stitching test is shown in Fig. 1. The green circle represents the reference surface, whereas the blue circle represents the surface under test. The shaded regions represent subapertures. The centre of the test surface is first measured and then the test surface is laterally shifted. The test surface is rotated through N equal angular intervals to generate a sufficient number of subapertures, while the reference surface is kept stationary. A central subaperture and a ring of subapertures are generated. In this case, W_C represents the measured data in the central subaperture and W_i (where $i = 1, 2, \ldots, N$) represents the measured data in the ring of subapertures.

2.1. Modified shift-rotation method

An interferometric measurement is mainly composed of the surface under test and the reference surface. The shift-rotation method involves general full-aperture absolute measurements. The surface map of an optical flat $T(x, y)$ can be decomposed into RS components $T^S(x, y)$ and RAS components $T^{AS}(x, y)$, which can be expressed as Eq. (1) [15].

$$T(x, y) = T^S(x, y) + T^{AS}(x, y) \tag{1}$$

To separate the reference and test surfaces, the shift-rotation method is further modified in SSI. The measured data in subapertures W_i and W_C are expressed as Eqs. (2) and (3).

$$W_i(x, y) = R(x, y) + T_i(x, y) = R + T^S(x, y) + T_i^{AS}(x, y) \tag{2}$$

$$W_C(x - t) = R(x, y) + T_C(x - t, y) = R + T^S(x - t, y) + T_C^{AS}(x - t, y) \tag{3}$$

where R represents the reference surface that is kept stationary during the test; T_i and T_C represent the surface map of the test surface in the ring of subapertures and the central subaperture, respectively. T_i^{AS} and T_C^{AS} represent the RAS components of the test surface in the ith subaperture and the central subaperture, respectively; The parameter t represents the lateral shift of the test surface. The RAS components of the test surface for each subaperture can be further calculated using Eq. (4), except the central subaperture.

$$\begin{aligned} W_i(x, y) - \frac{1}{N}\sum_{i=1}^{N} W_i(x, y) &= T_i^{AS}(x, y) - \frac{1}{N}\sum_{i=1}^{N}\left(T_i^{AS}(x, y)\right) \\ &= T_i^{AS}(x, y) - T_i^{kN\theta}(x, y) \end{aligned} \tag{4}$$

where $T_i^{kN\theta}$(x, y) is the test surface deviation of the $kN\theta$ order terms, $k = 1, 2, 3, \ldots$. Considering the $kN\theta$ order terms are usually small enough to be neglected, the $kN\theta$ order terms are excluded in our following simulations and experiments. The RS components of the test surface can be calculated from Eqs. (2) and (3) as shown in Eq. (5).

$$\begin{aligned} W_C(x - t, y) - W_i(x, y) = T^S(x - t, y) - T^S(x, y) + T_C^{AS}(x - t, y) \\ - T_i^{AS}(x, y) \end{aligned} \tag{5}$$

The least squares method is further used to calculate T^S, which is expressed as an even polynomial except the 2nd order term. However, the component T_C^{AS} cannot be obtained in the above process. To acquire the component T_C^{AS}, the maximum likelihood method is implemented without the auxiliary experimental process as detailed in Section 2.2.

Considering the diameter difference between the reference and test surfaces, a more complex but generalized arrangement of subapertures is considered, as shown in Fig. 2. Multiple shifts and rotations are carried out so that a central subaperture and several rings of subapertures are generated to test the surface's full aperture. The radial subapertures generated by shifts as shown in the red rectangle can be used to reconstruct the RS components of the test surface with Eq. (5). Each ring of subapertures generated by rotations is calculated using Eq. (4) to gain the RAS components of the test surface. We suppose that the modified shift-rotation method is suitable for different subaperture arrangements.

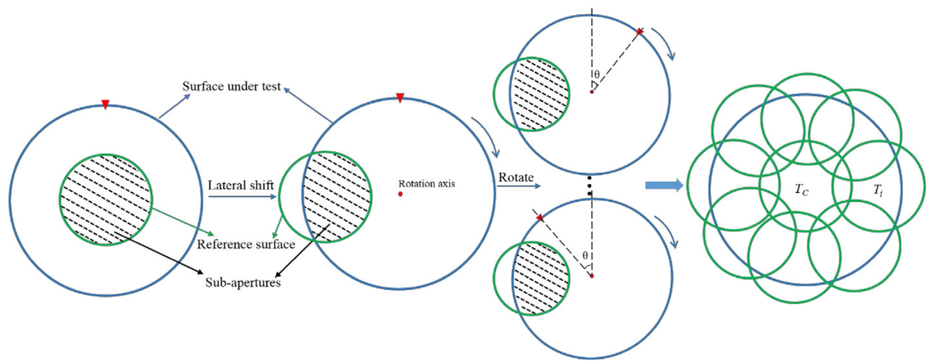

Fig. 1. Geometric setup of subaperture stitching test.

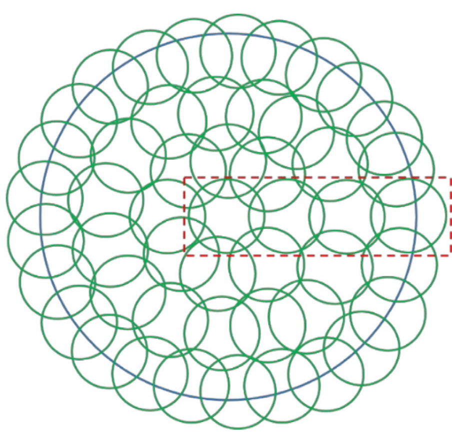

Fig. 2. Subaperture arrangement with multiple shifts and rotations.

2.2. Maximum likelihood method

For each subaperture measurement, the height differences between the reference and test surfaces are measured. The testing data can be expressed as shown in Eq. (6) [11].

$$\begin{aligned} D_{ij} = {} & D_{ij}^{T} + D_{ij}^{R} + D_{res} = P_i Z_1\left(\rho_a, \theta_a + \varphi_{ai}\right) + T_{xi} Z_2\left(\rho_a, \theta_a + \varphi_{ai}\right) \\ & + T_{yi} Z_3\left(\rho_a, \theta_a + \varphi_{ai}\right) \\ & + DE_i Z_4\left(\rho_a, \theta_a + \varphi_{ai}\right) - \sum_{k=5}^{rm} B_{rk} Z_k\left(\rho_b, \theta_b + \varphi_{bi}\right) \\ & + \sum_{k=5}^{tm} A_{tk} Z_k\left(\rho_a, \theta_a + \varphi_{ai}\right) + D_{res} \end{aligned} \tag{6}$$

where D_{ij} is the phase data of point j in the ith subaperture; D_{ij}^{R} and D_{ij}^{T} are the phase data of the reference and test surfaces, respectively; Z_k are Zernike polynomials that represent surfaces; P_i, T_{xi}, T_{yi} and DE_i are the mutual alignment errors, which are piston, tilt and defocus between the subapertures; *rm* and *tm* are the highest indexes of terms to describe the reference and test surfaces, respectively; B_{rk} and A_{tk} are Zernike coefficients of the reference and test surfaces, respectively; ρ, θ and φ are global coordinates of the reference and test surfaces in a subaperture; and D_{res} represents the residual phase value that cannot be described by the Zernike polynomials.

When the residual testing errors are small enough to be ignored, the likelihood function of a subaperture testing map can be written as Eq. (7) because the phase data of each subaperture meets the Gauss distribution.

$$L\left(A_{tk}, B_{rk} | D_{ij}\right) = \frac{1}{\left(\sqrt{2\pi\sigma}\right)^{NV_i}} exp(-\frac{1}{2\sigma^2} \sum_{i=1}^{N} \sum_{j=1}^{V_i} (D_{ij} - D_{ij}^{T} - D_{ij}^{R})^2) \tag{7}$$

where N represents the number of the testing subapertures and V_i represents the number of phase data in the ith subaperture.

The goal of the method is to obtain the Zernike coefficient A_{tk} of the test surface so that Eq. (8) is obtained by maximizing the logarithm of the likelihood function.

$$S = \sum_{i=1}^{N} \sum_{j=1}^{V_i} ((D_{ij} - D_{ij}^{T} - D_{ij}^{R})^2) = \min \tag{8}$$

$$T_C^{AS0} = \sum_{n=5}^{37} A_n Z_n\left(\rho_a, \theta_a\right), n \neq 11, 22 \tag{9}$$

The coefficients A_{tk} and B_{rk} can be obtained from Eq. (8) using the least squares method. Z_n denotes the RAS polynomials in the Zernike circle polynomials [16]. The coefficient A_n is a Zernike coefficient extracted from the coefficient A_{tk}. The component T_C^{AS0}, which lack of high-frequency components compared with T_C^{AS} mentioned in the above Section 2.1, can be reconstructed using Eq. (9). Moreover, the component T_C^{AS0} are used to calculate the RS components T^S of the test surface by Eq. (5). However, the high-frequency components in the central subaperture are abandoned, considering that the component T_C^{AS0} is constructed using Zernike coefficients. The surface map of the high-frequency central subaperture T_C is further obtained from Eq. (10). The surface maps of subapertures T_i are acquired by the sum of the components T^S and T_i^{AS}. The full surface map of the test surface is obtained from the stitching algorithm for all subapertures.

$$T_C = W_C - \frac{1}{N} \sum_{i=1}^{N} (W_i - T_i) \tag{10}$$

The flow chart of the proposed method is shown in Fig. 3. A sufficient number of subapertures are generated by the shift and rotation of the test surface. Then, the maximum likelihood method is applied to reconstruct the RAS components in the central subaperture T_C^{AS0} described by the Zernike polynomials. The RAS components in the ring of subapertures are calculated using Eq. (4). The RS components of the full aperture of the test surface are calculated using the subapertures 1 and 7 using Eq. (5). The surface maps of the ring of subapertures are acquired by summing the RAS components T_i^{AS} and the RS components T^S. The surface map of the central subaperture that maintains a high frequency is obtained using Eq. (10). Then, the stitching algorithm for subapertures T_i and T_C is implemented to obtain absolute measurements of the test surface.

3. Simulations

3.1. Comparison of the traditional stitching algorithm and the hybrid self-calibration method

The proposed method is validated by simulating two flat surfaces, in which the surface maps as shown in Fig. 4 are experimentally measured data. The reference surface cannot be ignored during the stitching

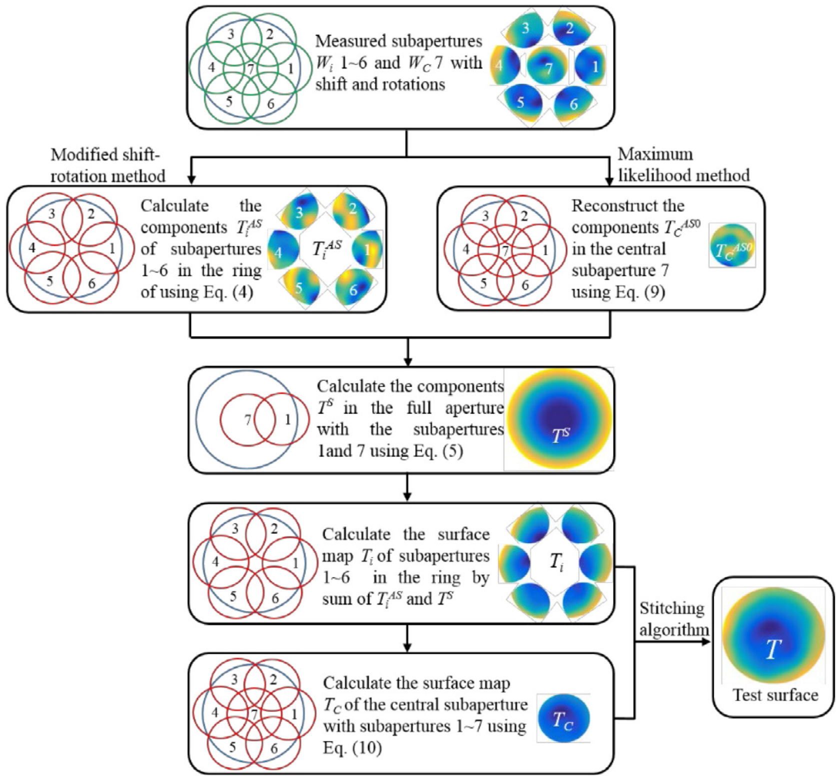

Fig. 3. Flow chart of the stitching algorithm.

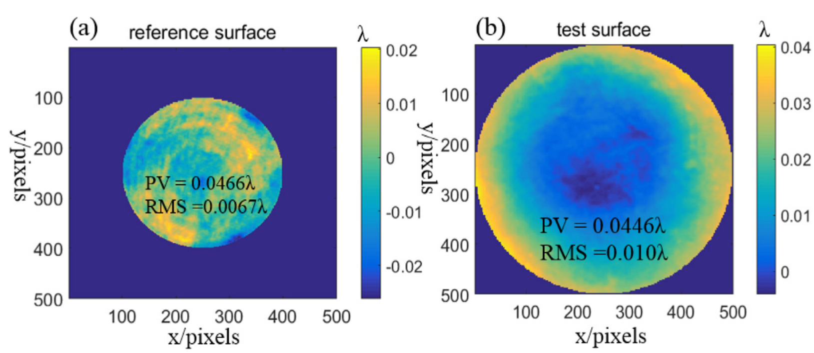

Fig. 4. Surface maps for simulations. (a) Reference surface; (b) Test surface.

process because the PV and RMS of the reference are 0.0466 λ and 0.0067 λ, respectively, which are close to those of the test surface—0.0446 λ and 0.01 λ, respectively. In Fig. 5, seven subapertures are artificially generated by shift and rotations of the test surface. The lateral shift is 180 pixels and the rotation angle step is 60°.

Fig. 6 shows the results of the test surface using the traditional stitching method without removing the reference surface and the stitched surface errors compared to the original test surface. The PV and RMS of the surface errors are 0.048 λ and 0.0072 λ, demonstrating that the low accuracy of the traditional stitching algorithm for the impacts of reference surface are non-ignorable. In addition, there are steps at the edges of the subapertures, as shown in Fig. 6.

The proposed method is also implemented by leveraging the above subapertures. The RAS components described by the Zernike polynomials are reconstructed by the maximum likelihood method, as shown in Fig. 7(a). Subsequently, the RS components are acquired with the central and shifted subapertures, as shown in Fig. 7(b). Further, the central region of the test surface is independently calculated using Eq. (10), while the high-frequency RAS components are calculated using Eq. (4). The stitched test surface is finally figured out after the calculation with Eq. (1) and stitching algorithm as shown in Fig. 7(c). The residual errors of the stitched test surface after point-to-point subtraction with the original test surface are shown in Fig. 7(d). The PV and RMS values of the residual errors are 0.0046 λ and 0.0005 λ, respectively, which demonstrate the high accuracy of the proposed method. The simulation errors are mainly derived from the $kN\theta$ order terms, which are neglected in the simulations. A practical method was proposed by Song to eliminate the $kN\theta$ order terms in the calculation of the RAS components [17]. In addition, the average of the high-frequency components in all subapertures is approximately equal to 0. Therefore, the residual high-frequency components also contribute to the simulation errors.

Furthermore, simulations utilizing QED's method are carried out for comparison with our proposed method. Fig. 8 shows the simulation results of the test surface using QED's method [9]. The surface form error of the reference surface is sufficiently eliminated during the

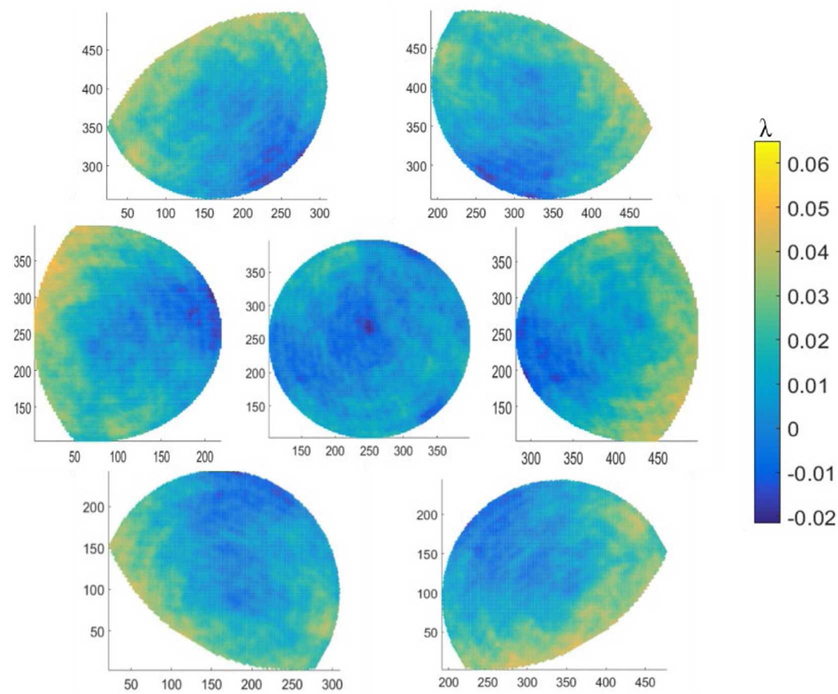

Fig. 5. Artificially generated subapertures.

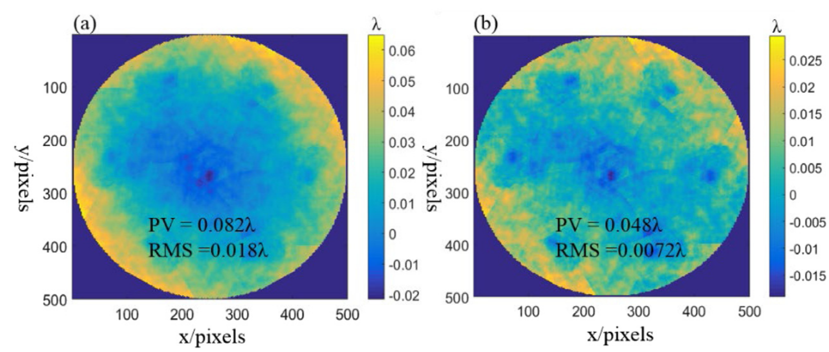

Fig. 6. Results of the test surface. (a) Surface map without removing reference surface; (b) Surface map of the residual errors.

stitching process, as shown in Fig. 8(a). The PV and RMS of the residual errors are 0.0189 λ and 0.0024 λ, respectively, as shown in Fig. 8(b). High-frequency components of the reference surface are coupled with the stitched test surface, which dominates the residual errors in the test surface. However, the high-frequency components of the reference surface are removed using our proposed method, which improves the accuracy of the stitching algorithm.

3.2. Analysis of positioning error

Lateral shift and rotations are inevitable mechanical movements when using the hybrid self-calibration method. Except for the common positioning errors caused by displacement and rotation angle errors, the tilt introduced by the shift affects the accuracy of the proposed method. The RS components of the test surface are calculated by the difference of the measured data before and after the lateral shift. For example, the difference in the pure power of the test surface $f(x, y) = x^2 + y^2$ before and after the shift by t is given as follows:

$$f(x + t, y) - f(x, y) = 2tx + t^2 \tag{11}$$

The x-tilt in the measured data is mixing with the power term when calculating the RS components of the test surface using the least squares method. The x-tilts with the maximum angle of $3 \times 10^{-4°}$ are added to the shifted subaperture, and then the stitching process is conducted. Residual errors are calculated by the difference between the stitching results and the original test surface. The PV and RMS results of the residual errors are shown in Fig. 9(a). The effects of the overlapping area of subapertures are simulated, with lateral displacement varying from 155 to 205 pixels. The corresponding results are shown in Fig. 9(b). The lateral shift and rotation angle errors with 10 pixels and 1° maximum, respectively, are also simulated. The corresponding results are shown in Fig. 9(c) and (d).

In Fig. 9(a), the PV values of the residual errors increase from 0.0046 λ to 0.024 λ when tilt occurs in the shifting process. In this way, the shifting mechanism should possess good linearity so that the tilt angle does not exceed $5 \times 10^{-5°}$, thereby guaranteeing the stitching accuracy. Therefore, the calculation accuracy of the power term through the subapertures before and after the displacement is restricted by the extremely high requirements for linearity of mechanism. The tilt induced by mechanism during the lateral displacement needs to be tested and then removed from the measured data to acquire the accurate power term of the test surface. The tilt testing method was proposed by Chen to calibrate the power induced by the reference

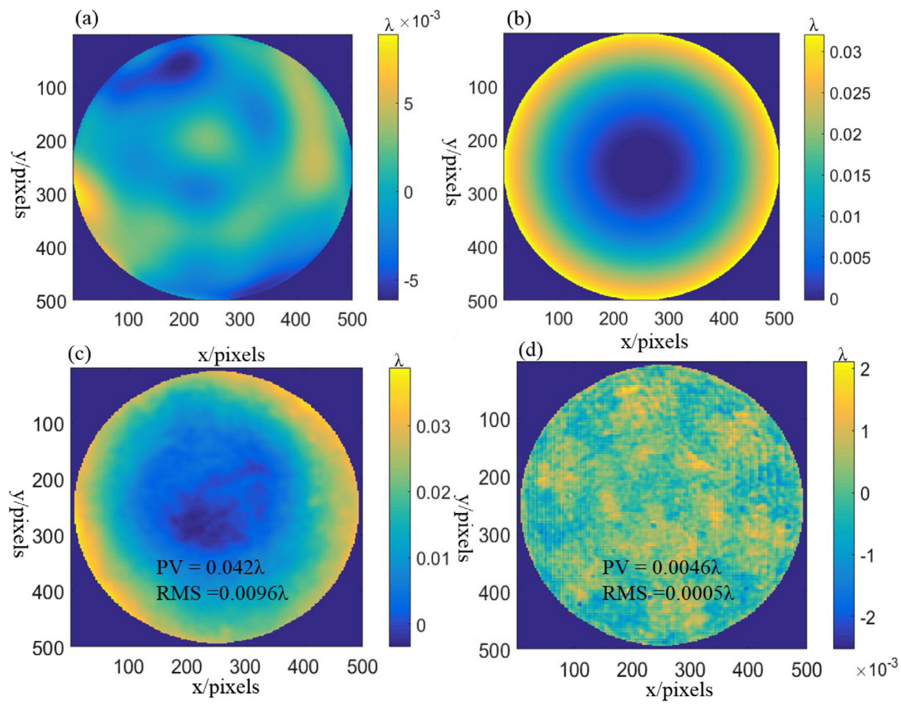

Fig. 7. Simulation results with the proposed method. (a) Rotationally asymmetric components of the test surface; (b) Rotationally symmetric components of the test surface; (c) Surface map of the test surface; (d) Surface map of the residual errors.

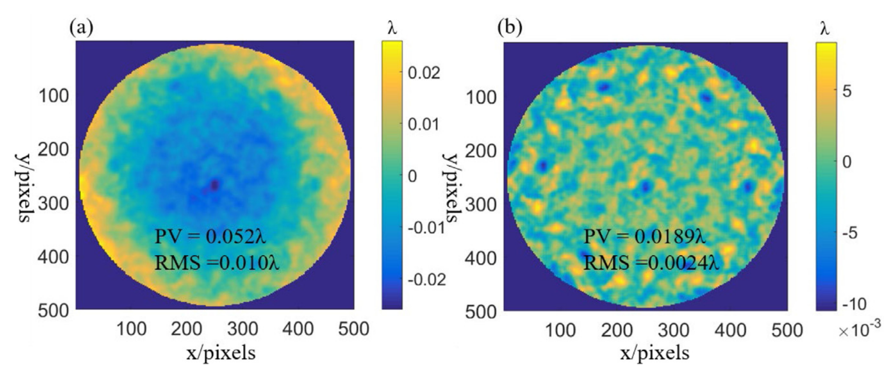

Fig. 8. Simulation results with QED's method. (a) Surface map of the test surface; (b) Surface map of the residual errors.

surface in subaperture stitching measurements [18]. In addition, the pentaprism scanning method and the three-flat testing method are commonly employed to obtain the power term of the test surface. The effects of the overlapping area are quite small as shown in Fig. 9(b), which demonstrates that the proposed method is insensitive to the overlapping area of subapertures. In Fig. 9(c), the stitching errors with PV = 0.016 λ and RMS = 0.0011 λ are introduced by displacement errors with 10 pixels maximum. However, many algorithms have been proposed to calibrate displacement errors up to the sub-pixel level. The rotation angle errors can be ignored as shown in Fig. 9(d) since the rotation accuracy of 1° can be easily realized.

4. Experimental results

To verify the feasibility of the proposed method, we performed experiments utilizing a 4-inch aperture commercial interferometer from Zygo Inc. A 60-mm iris is placed at the exit of the interferometer to simulate a 100-mm aperture flat mirror test by using a small-aperture interferometer. A six-dimensional mechanism was used to shift and rotate the test surface, as shown in Fig. 10. Although a horizontal interferometric system was adopted in the experiment, we supposed that the surface deformation induced by rotations could be neglected. Interferometric measurements at seven subapertures were implemented. The lateral displacement was 40 mm and the rotation angle step was 60°. The original interference fringes and the corresponding surface maps are shown in Fig. 11. The position deviations caused by the mechanism were calibrated using our previously published algorithm during the stitching process [19].

In Fig. 12(a) and (b), the RAS and the RS components of the test surface described by the Zernike polynomials are reconstructed using the maximum likelihood method. The test surface map described by the Zernike polynomials, as shown in Fig. 12(c), is acquired by the sum of the surface data in Fig. 12(a) and (b). Although the surface form error of the test surface is well extracted from the subapertures, the high-frequency components of the test surface are lost, decreasing the testing accuracy.

Full-aperture absolute measurements using the shift-rotation method were carried out to acquire the absolute surface map of the test surface.

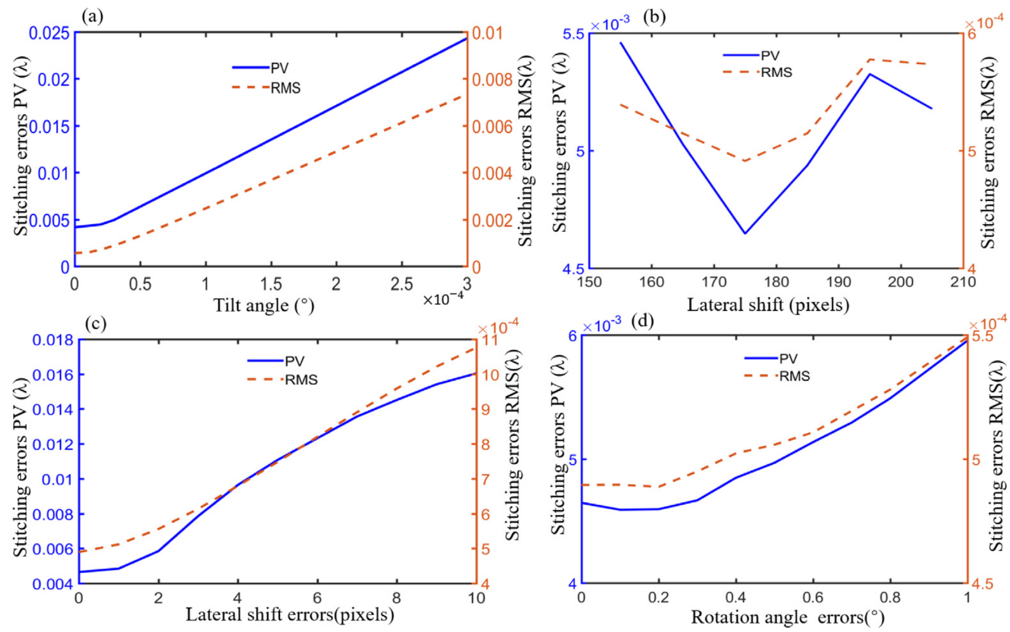

Fig. 9. Residual errors considering positioning error. (a) Residual errors induced by tilt angle in the shifting process; (b) Residual errors induced by varying lateral shift; (c) Residual errors induced by lateral shift errors; (d) Residual errors induced by rotation angle errors.

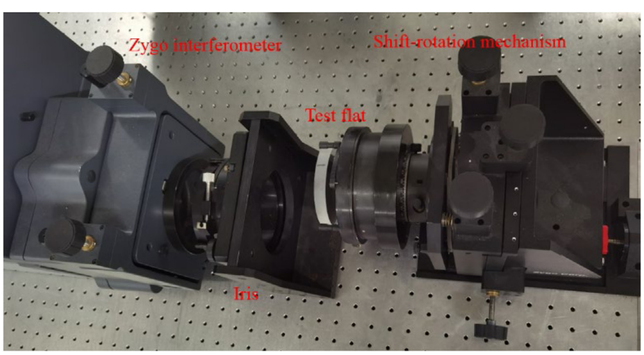

Fig. 10. Experimental setup.

The results are shown in Fig. 13(a), where PV is 0.111 λ and RMS is 0.018 λ.

The stitching results of the test surface utilizing QED's method are shown in Fig. 13(b), where PV and RMS are 0.105 λ and 0.021 λ, respectively. The stitching results of the test surface using our proposed method are shown in Fig. 13(c), where PV and RMS are 0.097 λ and 0.019 λ, respectively. Both the stitching results using QED's method and our proposed method are compared with the results using full-aperture absolute measurements. The corresponding residual errors are shown in Fig. 13(d) and (e). The PV and RMS of the residual errors using QED's method are 0.025 λ and 0.003 λ, respectively. The PV and RMS of the residual errors using our proposed method are 0.018 λ and 0.003 λ, respectively. The results of the proposed method are quite similar to those derived from QED's method. Considering the tiny high-frequency components of the reference surface compared to those of the surface map of the test surface, the stitching results using the proposed method and QED's method perform both well. Therefore, the residual errors of the proposed method demonstrate that the impacts of reference surface are well eliminated and that the surface details are precisely retained.

5. Conclusions

In this study, we proposed a hybrid self-calibration algorithm for subaperture testing of an optical flat, considering the impact of the reference surface. Subapertures are generated by shift and rotations of the test surface. In this case, we found the proposed method to be suitable for SSI with vertical interferometric system. The surface map of the reference surface is well eliminated in all subapertures. The test surface is accurately reconstructed by retrieving the RAS and RS components. Although the calculation of power of the test flat still needs auxiliary measurements, such as tilt testing during the lateral displacement, the pentaprism scanning method or the three-flat testing method, the impact of the reference surface can be eliminated with high accuracy in the stitching process using our proposed method. Both the simulation and experimental results confirm the feasibility of the proposed method. However, a limitation is that only flat mirrors were tested. Thus, future work will focus on the testing of spherical mirrors and more complex surfaces.

Declaration of competing interest

The authors declare that they have no known competing financial interests or personal relationships that could have appeared to influence the work reported in this paper.

Acknowledgements

We would like to thank the National Key Research and Development Program (2019YFB2005500); National Natural Science Foundation of China (62175107, U1931120); Six talent peaks project in Jiangsu Province, China (RJFW-019); Foundation of key laboratory of optical system advanced manufacturing technology, Chinese academy of sciences (KLOMT190201); and Foundation of Shanghai key laboratory of online test and control technology (ZX2021102) for their financial support.

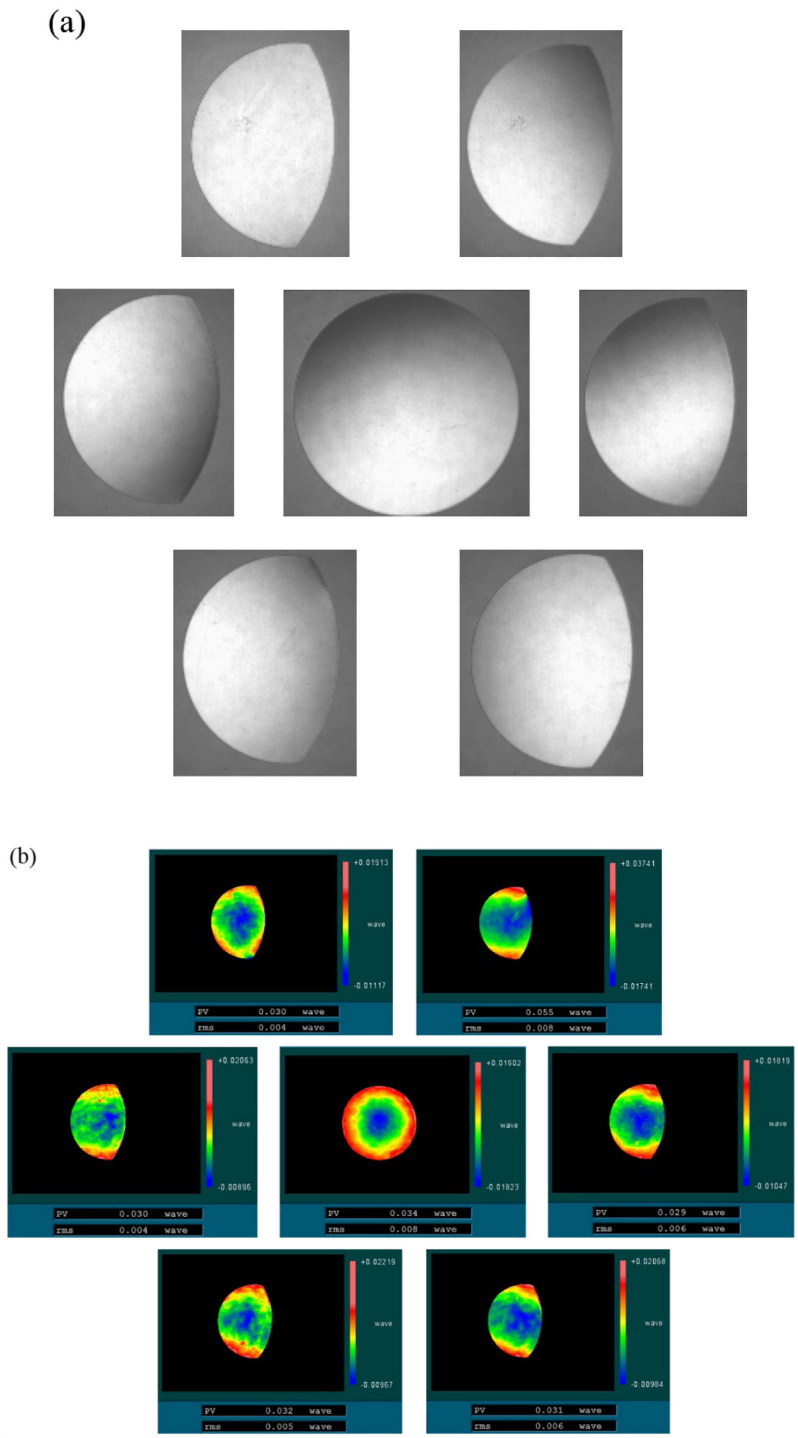

Fig. 11. Subaperture stitching testing of a 100-mm flat. (a) Interference fringes; (b) Surface maps of the all subapertures.

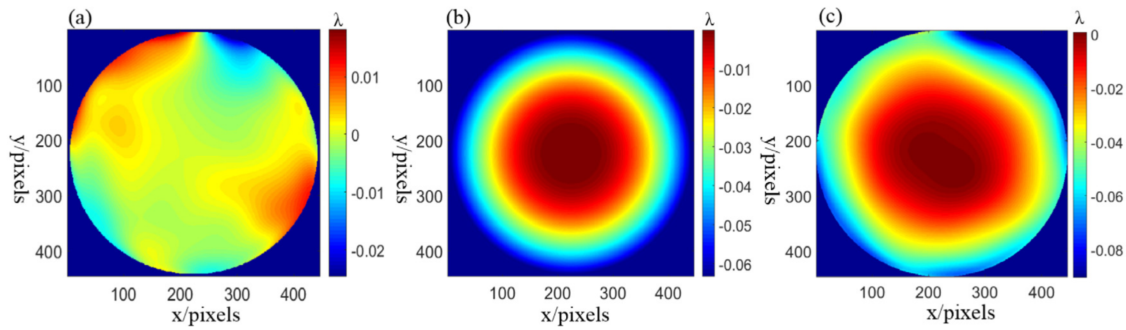

Fig. 12. Components of the test surface. (a) Rotationally asymmetric components; (b) Rotationally symmetric components; (c) Test surface described by Zernike polynomials.

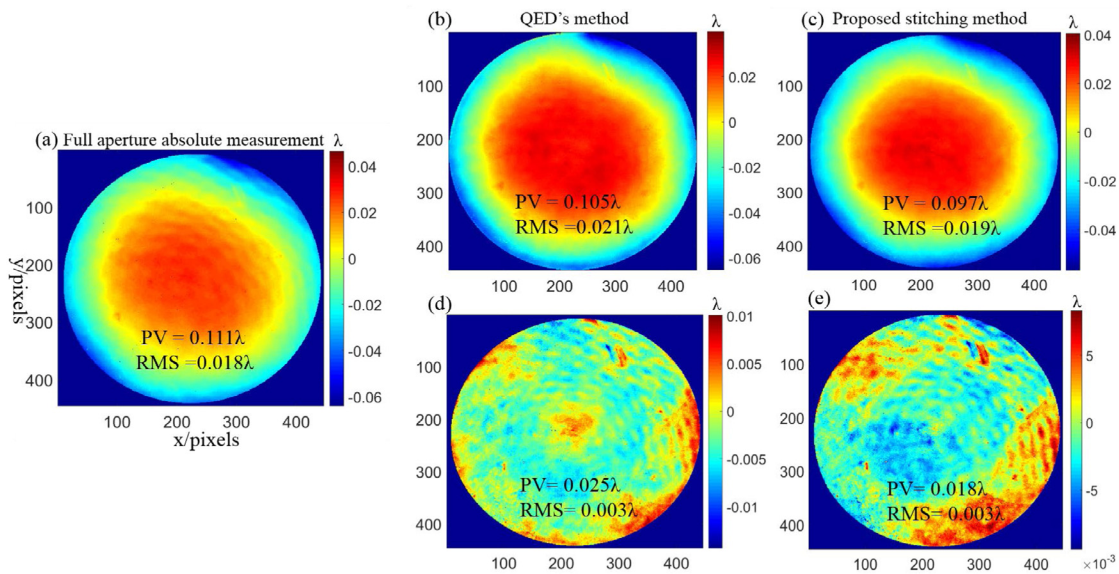

Fig. 13. Experimental results of the test surface. (a) Surface map utilizing full-aperture absolute measurement; (b) Surface map utilizing QED's method; (c) Surface map utilizing the proposed method; (d) Residual errors between (b) and (a); (e) Residual errors between (c) and (a).

References

[1] C.-J. Kim, J.C. Wyant, Subaperture test of a large flat on a fast aspheric surface, J. Opt. Soc. Amer. 71 (1981) 1587.

[2] R. Maurer, F. Schneider, C. Vogt, M. Schinhaerl, P. Sperber, R. Rascher, Physical marker based stitching process of circular and non-circular interferograms, Proc. SPIE 8083 (2011) 80830Q.

[3] P. Zhang, H. Zhao, X. Zhou, J. Li, Subaperture stitching interferometry using stereovision positioning technique, Opt. Express 18 (2010) 15216–15222.

[4] S. Tang, C. Brian, Measuring height variation over entire wafer surface with high lateral resolution, Proc. SPIE 6672 (2007).

[5] S.Y. Chen, S.Y. Li, Y.F. Dai, Iterative algorithm for subaperture stitching interferometry for general surfaces, J. Opt. Soc. Amer. A 22 (2005) 1929–1936.

[6] Ulf Griesmann, Three-flat test solutions based on simple mirror symmetry, Appl. Opt. 45 (2006) 5856–5865.

[7] Bernard S. Fritz, Absolute calibration of an optical flat, Opt. Eng. 23 (1984) 234379.

[8] Chiayu. Ai, James C. Wyant, Absolute testing of flats by using even and odd functions, Appl. Opt. 32 (1993) 4698–4705.

[9] QED Technologies Inc. Software Patent: Simultaneous self-calibrated subaperture stitching for surface figure measurement (interferometer) European patent EP1, 324, 006 (1 July 2003).

[10] P. Su, J. Burge, R.A. Sprowl, J. Sasian, Maximum likelihood estimation as a general method of combining subaperture data for interferometric testing, in: International Optical Design, Technical Digest (CD) (Optical Society of America), 2006, paper ThA2.

[11] Peng. Su, James H. Burge, Robert E. Parks, Application of maximum likelihood reconstruction of subaperture data for measurement of large flat mirrors, Appl. Opt. 49 (2010) 21–31.

[12] L. Yan, W. Luo, G. Yan, X. Wang, H. Zhang, L. Chao, D. Ma, X. Tang, Subaperture stitching testing for fine flat mirrors with large apertures using an orthonormal polynomial fitting algorithm, Opt. Lasers Eng. 120 (2019) 49–58.

[13] S. Chen, Y. Dai, S. Li, X. Peng, J. Wang, Error reductions for stitching test of large optical flats, Opt. Laser Technol. 44 (2012) 1543–1550.

[14] Goeun Kim, In-Ung Song, June Gyu Park, Hagyong Kihm, Ho-Soon Yang, Dual subaperture stitching for large flat mirror testing, Appl. Opt. 59 (2020) 8681–8687.

[15] Weihong Song, Fan Wu, Xi Hou, Yongjian Wan, Optimized absolute testing method of shift-rotation, Appl. Opt. 52 (2013) 7028–7032.

[16] D. Malacara, Optical Shop Testing, third ed., Wiley, 2007.

[17] Weihong Song, Fan Wu, Xi Hou, Yongjian Wan, Optimized absolute testing method of shift-rotation, Appl. Opt. 52 (2013) 7028–7032.

[18] Shanyong Chen, Chuanchao Wu, Guipeng Tie, Dede Zhai, Stitching test of large flats by using two orthogonally arranged wavefront interferometers, Appl. Opt. 56 (2017) 9193–9198.

[19] Ruoyan Wang, Zhishan Gao, Dan Zhu, Weijian Liu, Wen Ji, Zhenyan Guo, Dasen Wang, Lingjie Wang, Yao Xu, Qun Yuan, Subaperture stitching interferometry based on the combination of the phase correlation and iterative gradient methods, Appl. Opt. 59 (2020) 4176–4182.